Low-Mass Galaxies at High Redshift

https://doi.org/10.1017/S1743921318007494 Published online by Cambridge University Press

Dwarf Galaxies: From the Deep Universe to the Present
Proceedings IAU Symposium No. 344, 2019
K. B. W. McQuinn & S. Stierwalt, eds.

doi:10.1017/S1743921318007494

Dwarf Galaxies: From the Epoch of Peak Star Formation to the Epoch of Reionization

Hakim Atek

Institut d'astrophysique de Paris, CNRS UMR7095, Sorbonne Université, 98bis Boulevard Arago, F-75014, Paris, France
email: hakim.atek@iap.fr

Abstract. Dwarf galaxies represent the dominant population at high redshift and they most likely contributed in great part to star formation history of the Universe and cosmic reionization. The importance of dwarf galaxies at high redshift has been mostly recognized in the last decade due to large progress in observing facilities allowing deep galaxy surveys to identify low-mass galaxies. This population appear to have extreme emission lines and ionizing properties that challenge stellar population models. Star formation follows a stochastic process in these galaxies, which has important implication on the ionizing photon production and its escape fraction whose measurements are challenging for both simulations and observations. Outstanding questions include: what are the physical properties at the origin of such extreme properties? What are the smallest dark matter halos that host star formation? Are dwarf galaxies responsible for cosmic reionization?

Keywords. galaxies: high-redshift, galaxies: formation, galaxies: evolution, galaxies: dwarf, (cosmology:) early universe

1. Introduction

The importance of dwarf galaxies is related to two of the most important periods in the history of the Universe. Firstly, the galaxy ultraviolet (UV) luminosity function (LF) at $z \sim 1-3$ shows that faint galaxies are the main contributors to the UV emission (e.g. Alavi *et al.* 2016), hence to the star formation density. This redshift range corresponds to the most efficient epoch in terms of star formation, where most of the stellar mass known today was formed (Madau & Dickinson 2014). Secondly, the UV LF at $z > 6$ and their ionizing properties show that dwarf galaxies most likely produced most of the ionizing emission responsible for cosmic reionization.

Overall, recent progress in observational facilities has allowed us to identify low-mass galaxies at high redshift, revealing their prevalence and their extreme properties compared to local galaxies and the massive counterparts. Dwarf galaxies are not the exception. They are the dominant population at high redshift. They are representative of the galaxy population and are therefore the best targets to understand the galaxy formation and evolution across cosmic time and the process of cosmic reionization.

2. Detecting Low-mass Galaxies at High Redshift

Until recently, our knowledge on the physical properties and the evolution of galaxies at high redshift was essentially based on samples of relatively massive galaxies. The photometric selection techniques used in deep galaxy surveys are biased towards bright-continuum galaxies. While narrow-band or spectroscopic surveys of the rest-frame ultraviolet (UV) domain have produced large samples of Lyman-alpha emitters at $z > 2$ (e.g. Drake *et al.* 2017, Sobral *et al.* 2018), their physical properties remain elusive due

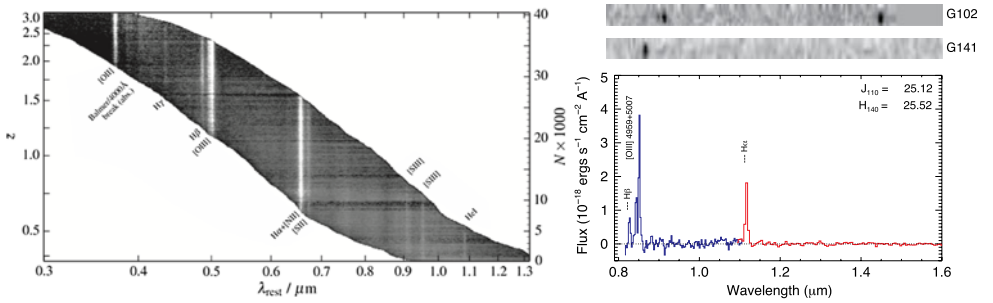

Figure 1. Slitless spectroscopy using the HST/WFC3 infrared grisms. **Left:** a montage of 1D spectra from Momcheva *et al.* (2016) shows the wavelength coverage of the G141 grism and the optical emission lines available as a function of redshift in the 3DHST survey. **Right:** 1D and 2D spectra from the WSIP survey (Atek *et al.* 2010) using both G102 and G141 grisms showing the detection of an extreme emission line galaxy with undetected stellar continuum.

to the lack of rest-frame optical emission lines which are redshifted to the near-infrared (NIR) window at high redshift. In order to overcome the strong atmospheric NIR airglow, several space-based spectroscopic programs have been conducted during the last decade, utilizing the powerful capabilities of the Wide Field Camera 3 (WFC3) onboard the *Hubble Space Telescope* (*HST*). The WFC3 NIR grisms slitless spectrocopy has been extensively used by the 3DHST survey (Brammer *et al.* 2012; Momcheva *et al.* 2016, Figure 1) and the pure-parallel program WISPS (Atek *et al.* 2010; see also Straughn *et al.* 2011). Such observations enabled the detection of pure emission lines (cf. Figure 1), regardless of their stellar continua, which led to the discovery of extremely strong emission line galaxies (e.g., Atek *et al.* 2011, Shim *et al.* 2011, see also Van der Wel *et al.* 2011) with equivalent widths reaching EW=1500 Å and stellar masses down to 10^8 $M_\odot$. While they remain relatively rare in the local Universe, such extreme objects are much more numerous at $z \sim 2$ and their prevalence seem to increase with redshift (Atek *et al.* 2011, Shim *et al.* 2011, Fumagalli *et al.* 2012, Stark *et al.* 2013, Schenker *et al.* 2013a, Smit *et al.* 2014). More recently, combining high sensitivity and high multiplexing, the multi-unit spectroscopic explorer (MUSE) on the VLT reached unprecedented discovery space, identifying emission lines galaxies that show no detection in the deepest HST images (e.g. Bacon *et al.* 2015, Maseda *et al.* 2018).

The strong gravitational lensing offered by massive galaxy clusters is a powerful tool to push further down the detection limits of current observing facilities. An important sample of ultra-faint dwarf galaxies has been detected at $z = 1 - 3$ behind lensing clusters, down to unprecedented magnitude limits of $M_{\rm UV} \sim -13$ mag (Alavi *et al.* 2016) using deep HST imaging in the UV. Similarly, the Frontier Fields Initiative (HFF) extended the galaxy UV luminosity function at $z \sim 6$ nearly three magnitudes deeper than the deepest HST observations of blank fields (Atek *et al.* 2015, Bouwens *et al.* 2017, Livermore *et al.* 2017, Ishigaki *et al.* 2018). Space- and ground-based spectroscopic observations of lensing clusters also allowed spatially-resolved studies of the physical properties of low-mass galaxies at high-redshift (Jones *et al.* 2015, Smit *et al.* 2017).

3. A New Look at Scaling Relations

The great progress in observing capabilities and strategies now shed a new light on some of the fundamental galaxy scaling relations. A tight correlation between the SFR and stellar mass at a given redshift has been observed at low and high redshift (e.g. Brinchmann *et al.* 2004, Noeske *et al.* 2007, Karim *et al.* 2011, Whitaker *et al.* 2012,

https://doi.org/10.1017/S1743921318007494 Published online by Cambridge University Press

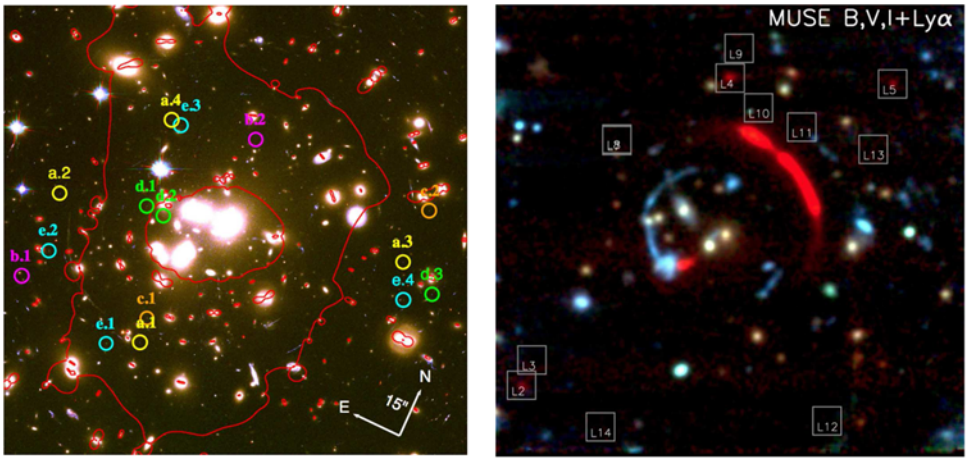

Figure 2. Lensing-assisted observations of dwarf galaxies at high redshift. **Left:** Multiple images of dwarf galaxies at $z \sim 1-3$ behind the massive galaxy cluster Abell 1689 from Alavi *et al.* (2016). The red curve denotes the critical line at $z = 2.5$. **Right:** A giant lensing arc of a galaxy at $z = 4.88$, behind the massive cluster RCS 0224, observed in Lyα with VLT/MUSE (Smit *et al.* 2017).

Speagle *et al.* 2014, Ilbert *et al.* 2014, Santini *et al.* 2017, Bisigello *et al.* 2018) describing a linear mass buildup in galaxies refereed to as the "main sequence". The slope, the normalisation, and the scatter of the SFR-M$_\star$ relation carry important information regarding the different processes that shape galaxies such as the gas accretion rate and the stochasticity of star formation activity. For this reason, various hydrodynamical simulations (Davé *et al.* 2011a, Torrey *et al.* 2014, Sparre *et al.* 2015, Tacchella *et al.* 2016, Matthee & Schaye 2018) and semi-analytical models (e.g., Dekel *et al.* 2013) attempted to reproduce the parameters of the main sequence but failed to fit the normalization and its evolution with redshift. Most of the constraints obtained on the SFR-M$_\star$ relation are restricted to the high-mass end and suffer from inconsistent measurements of the SFR. Such studies also rely on photometric redshifts due to the lack of spectroscopic information. Recent spectroscopic programs enables the exploration of larger dynamical range in stellar masses going down to M$_\star \sim 10^7$M$_\odot$ and direct measurements of the SFR using the Hα emission line. Figure 3 shows the SFR-M$_\star$ relation for EELGs and how they compare to the rest of emission-line galaxies and how they show a large offset from the "main sequence", which denotes the starbursting nature of these low-mass galaxies (Atek *et al.* 2014c). During each starburst episode the galaxy departs from the main sequence. Hydrodynamical simulations of dwarf galaxies have successfully reproduced the stochastic star formation, showing in particular that each star formation episode is triggered by gas accretion before supernova outflows deplete the central region of gas. A succession of gas accretion from the halo leads to a highly stochastic star formation activity (Governato *et al.* 2012, Shen *et al.* 2014, Madau *et al.* 2014, Sparre *et al.* 2017). A direct consequence of this burstiness is a larger dispersion in the observed SFR indicators, such as the Hα line, in lower-mass galaxies. Therefore, galaxy surveys targeting the Hα equivalent width, will miss a significant fraction of star-forming dwarfs (Dominguez *et al.* 2015).

The stellar mass buildup in galaxies also leads to chemical enrichment of their interstellar medium (ISM). Therefore, the relation between the gas phase metallicity and the SFR or stellar mass is an important test for galaxy evolution models (Peeples & Shankar 2011, Lilly *et al.* 2013, Chisholm *et al.* 2018,) as it describes the interplay between neutral

https://doi.org/10.1017/S1743921318007494 Published online by Cambridge University Press

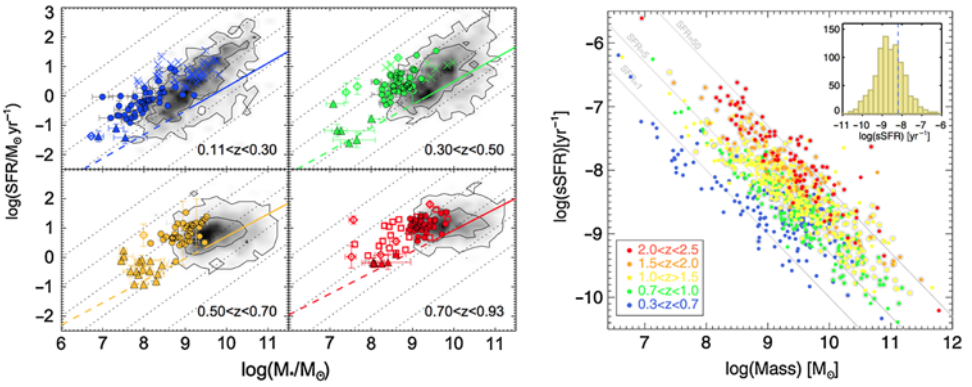

Figure 3. The star formation rate and stellar mass relation. **Left:** SFR-M$_\star$ for EELGs compared to star-forming galaxies at four different redshifts (Amorin *et al.* 2015). The solid and dashed lines represent the main sequence at the corresponding redshifts from Whitaker *et al.* 2012. **Right:** The specific SFR vs stellar mass for grism-selected EELGs from $z = 0.3$ to $z = 2.5$ from Atek *et al.* (2014).

gas accretion, which dilutes metals, and the outflowing metal-rich gas. On the observational side, the oxygen abundance is found to correlate with the stellar mass (MZR) and its normalization also evolves with redshift (Tremonti *et al.* 2004, Maiolino *et al.* 2008, Berg *et al.* 2012, Troncoso *et al.* 2014, Zahid *et al.* 2014). However, extending the MZR to lower stellar masses (below 10^9 M$_\odot$) at high redshift is challenging, and the slope or the normalization are still poorly constrained (Henry *et al.* 2013, Whitaker *et al.* 2014, Salim *et al.* 2014). Recently, the gas-phase metallicity has been measured in a sample of low-mass EELGs at $z \sim 3$ and shows a strong evolution towards low metallicities compared to more massive galaxies at similar redshifts (Amorin *et al.* 2017). If the burst episodes in these dwarfs are fuelled by gas accretion, then their large offset from the MZR can be explained by the inflow of metal-poor gas. HST imaging of these galaxies also reveal very small sizes, hence very high SFR surface densities. Spectroscopic observations of a similar population of galaxies at $1.3 < z < 2.3$ show a high star formation efficiency with a mass growth scale of ~ 10 Myr (Maseda *et al.* 2014, Atek *et al.* 2014).

4. Dwarf Galaxies at the Epoch of Reionization

Cosmic reionization is one of the most important transitions in the history of the Universe. It corresponds to the global ionization of the neutral hydrogen in the Universe by the first sources of light that happened between $z \sim 6$ and $z \sim 10$ (Fan *et al.* 2006, Becker & Bolton 2013, Planck Collaboration 2016). Identifying the sources responsible for cosmic reionization remains a major challenge in observational cosmology. While there is still no consensus on the nature of these sources, most recent studies point towards early star-forming galaxies as the main sources of the UV emission, hence most likely the ionizing emission (e.g. Robertson *et al.* 2015, Bouwens *et al.* 2015, Finkelstein *et al.* 2015). In order to assess the exact contribution of galaxies to the ionizing background, one needs to measure three main quantities: the non-ionizing UV luminosity density, the ionizing photon production efficiency relative the UV emission, and the escape fraction of ionizing radiation from galaxies. The integrated UV luminosity density depends on the shape of the UV luminosity function of galaxies, particularly at the faint end where it becomes vey steep, and where it reaches the smallest galaxies even formed, i.e. the faint integration limit. Galaxy deep blank fields surveys with *HST* have put strong constraints on the overall shape of the UV LF with more than a thousand of galaxies identified at $z > 6$ (Bunker *et al.* 2010; Oesch *et al.* 2010, Bouwens *et al.* 2011, Finkelstein *et al.* 2012,

https://doi.org/10.1017/S1743921318007494 Published online by Cambridge University Press

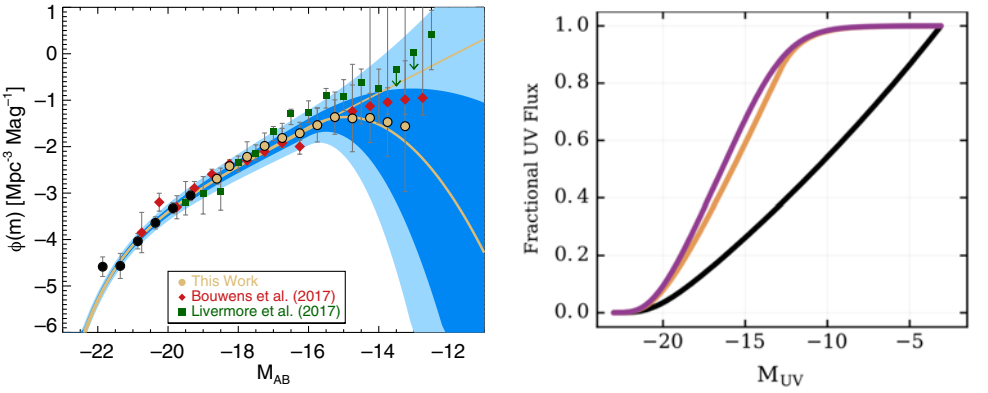

Figure 4. The galaxy UV luminosity function at $z \sim 6$ using gravitational lensing. **Left:** The UV LF from the Frontier Fields observations and the best fit using a modified form of the Schechter function allowing for a rollover at the fain end (Atek *et al.* 2018). The dark and light regions show the significant uncertainties on the shape of the UV LF beyond $M_{UV} \sim -15$ AB. **Right:** The cumulative contribution of galaxies as a function of their absolute UV magnitude in the case of a steep faint-end slope (black line) and in the case of a turnover around $M_{UV} = -13$ AB (orange and purple lines) from Weisz *et al.* (2017).

McLure *et al.* 2013, Schenker *et al.* 2013a, Bouwens *et al.* 2015). The very steep faint-end slope of the UV LF ($\alpha \sim -2$) clearly demonstrates that dwarf galaxies are likely the dominant contributor to the total UV emission. However, the integrated UV luminosity density falls short of the required threshold to maintain the IGM ionized, which calls for a contribution for fainter galaxies beyond the detection limits of blank field surveys around $M_{UV} \sim -17$ AB.

The strong gravitational lensing offered by massive galaxy clusters offer a unique opportunity to push the detection limits of current instrumentation by amplifying the flux of distant background sources (Kneib & Natarajan 2011, Sharon *et al.* 2012, Postman *et al.* 2012, Richard *et al.* 2014, Salmon *et al.* 2017). The Hubble Frontier Fields program (Lotz *et al.* 2017), which consists of deep multi-band imaging of six massive clusters, has enabled the identification of extremely faint galaxies and constraints on the UV LF more than two magnitudes deeper than previous studies (Atek *et al.* 2014b, Atek *et al.* 2015a,b, Ishigaki *et al.* 2014, Zheng *et al.* 2014, Yue *et al.* 2014, Castellano *et al.* 2016; Laporte *et al.* 2016, Bouwens *et al.* 2017, Livermore *et al.* 2017, Kawamata *et al.* 2018). These results confirm a steep faint-end slope of $\alpha \sim -2$ down to an intrinsic magnitude of $M_{\rm UV} \sim -15$ (see Figure 4, left). Beyond this limit, uncertainties become too important to reliably identify a rollover at the faint end of the UV LF, as the discrepancies observed between different studies reveal. The right panel of Figure 4 shows the cumulative contribution of galaxies as a function of their intrinsic magnitude (Weisz *et al.* 2017). In the case of a steep faint-end slope, the contribution of fainter galaxies keep increasing with more than 60% of the UV emission coming from galaxies fainter than $M_{\rm UV}$= -15. When the UV LF rolls over around $M_{\rm UV}$= -13, the contribution of these ultra-faint galaxies is only about 30%.

Also regarding the faint end of the UV LF, near-field studies have produced independent constraints by local dwarfs as fossils of high-redshift galaxies. Combining their star formation histories with stellar population models offer another perspective on their progenitors at early times, predicting a steep faint-end slope out to $z \sim 5$ (Weisz *et al.* 2015). The most notable result of of such studies shows that there should be a turnover in the UV LF at $z \sim 6$ approximately around $M_{\rm UV}$= -13 (Boylan-Kolchin *et al.* 2015).

https://doi.org/10.1017/S1743921318007494 Published online by Cambridge University Press

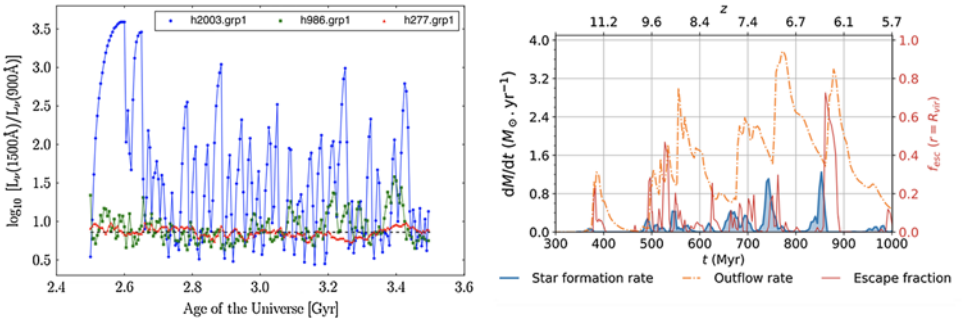

Figure 5. The ionizing emissivity of dwarf galaxies. *Left:* The ionizing efficiency of three simulated dwarf galaxies with stellar masses $\log(M_\star/M_\odot)$=7 (blue line), 8.5 (green line), and 10 (red line) from Dominguez *et al.* (2014). The stasr formation stochasticity on the low-mass galaxy leads to large variation in the ionizing efficiency, with an average value significantly higher than other galaxies. **Right:** evolution of the escape fraction of ionizing radiation compared to the star formation and the outflows rates in simulated galaxies from Trebitsch *et al.* (2017). After each SF burst episode the escape fraction increases following the outflow rate.

A steep faint-end slope that extends to magnitudes fainter than $M_{\rm UV} = -13$ would lead to an overproduction of dwarf galaxies in the local Universe.

Assuming canonical values for the ionizing radiation efficiency and escape fraction (log $f_{esc}\xi_{ion}$ = 24.53), The derived UV luminosity density at $z \sim 6$ in the Frontier Fields results, although lower than previous determinations due to the potential turnover, is still in agreement with the required emissivity to maintain reionization. However, the precise measurement of the ionizing efficiency and its escape fraction of the dominant population of dwarf galaxies are necessary to determine their contribution to the ionizing background. The stochastic nature of star formation in low-mass galaxies have important implications on these parameters. Hydrodynamical simulations show that the bursty star formation lead to strong variations on a short timescale of the ionizing emissivity (e.g. Dominguez *et al.* 2015). The average ratio between the ionizing and the non-ionizing continuum luminosities L_ν(900 Å)/L_ν1500 Å becomes significantly higher than the constant value of 7 usually assumed for a constant star formation (Figure 5). High-resolution simulations also show that each burst episode is followed by supernova-driven outflows that clear the ISM and facilitates the escape of ionizing radiation (Trebitsch *et al.* 2017). The knowledge of the duty cycle and the physical properties regulating the production and the escape of ionizing radiation is still challenging in hydro zoom-in simulations but also in observations. Indirect measurements of ξ_{ion} at $z \sim 4-5$ have been recently been reported using IRAC flux excess to derive the Hα flux and infer the ionizing photon production rate (Bouwens *et al.* 2016). More direct spectroscopic measurements at $z \sim 2$ show higher ξ_{ion} values in galaxies with a blue UV slope similar to $z > 6$ galaxies, although with a large scatter (Shivaei *et al.* 2018). Large spectroscopic surveys combined with deep UV observations are needed to make progress regarding these two important parameters.

References

Amorín, R., Fontana, A., Pérez-Montero, E., *et al.* 2017, *Nature Astronomy*, 1, 0052
Amorín, R., Pérez-Montero, E., Contini, T., *et al.* 2015, *A&A*, 578, A105
Atek, H., Richard, J., Kneib, J.-P., & Schaerer, D. 2018, *MNRAS*, 479, 5184
Atek, H., Richard, J., Jauzac, M., *et al.* 2015, *ApJ*, 814, 69
Atek, H., Richard, J., Kneib, J.-P., *et al.* 2015, *ApJ*, 800, 18
Atek, H., Kneib, J.-P., Pacifici, C., *et al.* 2014, *ApJ*, 789, 96

https://doi.org/10.1017/S1743921318007494 Published online by Cambridge University Press

Atek, H., Richard, J., Kneib, J.-P., *et al.* 2014, *ApJ*, 786, 60
Atek, H., Siana, B., Scarlata, C., *et al.* 2011, *ApJ*, 743, 121
Atek, H., Malkan, M., McCarthy, P., *et al.* 2010, *ApJ*, 723, 104
Becker, G. D., & Bolton, J. S. 2013, *MNRAS*, 436, 1023
Bisigello, L., Caputi, K. I., Grogin, N., & Koekemoer, A. 2018, *A&A*, 609, A82
Bacon, R., Brinchmann, J., Richard, J., *et al.* 2015, *A&A*, 575, A75
Boylan-Kolchin, M., Weisz, D. R., Johnson, B. D., *et al.* 2015, *MNRAS*, 453, 1503
Bouwens, R. J., Oesch, P. A., Illingworth, G. D., Ellis, R. S., & Stefanon, M. 2017, *ApJ*, 843, 129
Bouwens, R. J., Smit, R., Labbé, I., *et al.* 2016, *ApJ*, 831, 176
Bouwens, R. J., Illingworth, G. D., Oesch, P. A., *et al.* 2015, *ApJ*, 811, 140
Bouwens, R. J., Illingworth, G. D., Oesch, P. A., *et al.* 2011, *ApJ*, 737, 90
Brammer, G. B., van Dokkum, P. G., Franx, M., *et al.* 2012, *ApJS*, 200, 13
Brinchmann, J., Charlot, S., White, S. D. M., *et al.* 2004, *MNRAS*, 351, 1151
Bunker, A. J., Wilkins, S., Ellis, R. S., *et al.* 2010, *MNRAS*, 409, 855
Castellano, M., Yue, B., Ferrara, A., *et al.* 2016, *ApJL*, 823, L40
Chisholm, J., Tremonti, C., & Leitherer, C. 2018, *MNRAS*,
Davé, R., Oppenheimer, B. D., & Finlator, K. 2011, *MNRAS*, 415, 11
Davé, R., Finlator, K., & Oppenheimer, B. D. 2011, *MNRAS*, 416, 1354
Domínguez, A., Siana, B., Brooks, A. M., *et al.* 2015, *MNRAS*, 451, 839
Drake, A. B., Garel, T., Wisotzki, L., *et al.* 2017, *A&A*, 608, A6
Fan, X., Strauss, M. A., Becker, R. H., *et al.* 2006, *AJ*, 132, 117
Finkelstein, S. L., Ryan, R. E., Jr., Papovich, C., *et al.* 2015, *ApJ*, 810, 71
Finkelstein, S. L., Papovich, C., Salmon, B., *et al.* 2012, *ApJ*, 756, 164
Fumagalli, M., Patel, S. G., Franx, M., *et al.* 2012, *ApJL*, 757, L22
Governato, F., Zolotov, A., Pontzen, A., *et al.* 2012, *MNRAS*, 422, 1231
Ilbert, O., Arnouts, S., Le Floc'h, E., *et al.* 2015, *A&A*, 579, A2
Ishigaki, M., Kawamata, R., Ouchi, M., *et al.* 2018, *ApJ*, 854, 73
Jones, T., Wang, X., Schmidt, K. B., *et al.* 2015, *AJ*, 149, 107
Kawamata, R., Ishigaki, M., Shimasaku, K., *et al.* 2018, *ApJ*, 855, 4
Kneib, J.-P., & Natarajan, P. 2011, *A&ARv*, 19, 47
Karim, A., Schinnerer, E., Martínez-Sansigre, A., *et al.* 2011, *ApJ*, 730, 61
Kurczynski, P., Gawiser, E., Acquaviva, V., *et al.* 2016, *ApJL*, 820, L1
Laporte, N., Infante, L., Troncoso Iribarren, P., *et al.* 2016, *ApJ*, 820, 98
Lilly, S. J., Carollo, C. M., Pipino, A., Renzini, A., & Peng, Y. 2013, *ApJ*, 772, 119
Livermore, R. C., Finkelstein, S. L., & Lotz, J. M. 2017, *ApJ*, 835, 113
Lotz, J. M., Koekemoer, A., Coe, D., *et al.* 2017, *ApJ*, 837, 97
Madau, P., Weisz, D. R., & Conroy, C. 2014, *ApJL*, 790, L17
Madau, P., & Dickinson, M. 2014, *ARA&A*, 52, 415
Maseda, M. V., Bacon, R., Franx, M., *et al.* 2018, arXiv:1809.01142
Maseda, M. V., van der Wel, A., Rix, H.-W., *et al.* 2014, *ApJ*, 791, 17
Matthee, J., & Schaye, J. 2018, arXiv:1805.05956
Momcheva, I. G., Brammer, G. B., van Dokkum, P. G., *et al.* 2016, *ApJS*, 225, 27
McLure, R. J., Dunlop, J. S., Bowler, R. A. A., *et al.* 2013, *MNRAS*, 432, 2696
Noeske, K. G., Weiner, B. J., Faber, S. M., *et al.* 2007, *ApJL*, 660, L43
Oesch, P. A., Bouwens, R. J., Illingworth, G. D., *et al.* 2010, *ApJL*, 709, L16
Peeples, M. S., & Shankar, F. 2011, *MNRAS*, 417, 2962
Pirzkal, N., Malhotra, S., Ryan, R. E., *et al.* 2017, *ApJ*, 846, 84
Planck Collaboration, Adam, R., Aghanim, N., *et al.* 2016, *A&A*, 596, A108
Postman, M., Coe, D., Benítez, N., *et al.* 2012, *ApJS*, 199, 25
Richard, J., Jauzac, M., Limousin, M., *et al.* 2014, *MNRAS*, 444, 268
Robertson, B. E., Ellis, R. S., Furlanetto, S. R., & Dunlop, J. S. 2015, *ApJL*, 802, L19
Salmon, B., Coe, D., Bradley, L., *et al.* 2017, arXiv:1710.08930
Santini, P., Fontana, A., Castellano, M., *et al.* 2017, *ApJ*, 847, 76

https://doi.org/10.1017/S1743921318007494 Published online by Cambridge University Press

Shen, S., Madau, P., Conroy, C., Governato, F., & Mayer, L. 2014, *ApJ*, 792, 99
Shim, H., Chary, R.-R., Dickinson, M., *et al.* 2011, *ApJ*, 738, 69
Sobral, D., Santos, S., Matthee, J., *et al.* 2018, *MNRAS*, 476, 4725
Schenker, M. A., Ellis, R. S., Konidaris, N. P., & Stark, D. P. 2013, *ApJ*, 777, 67
Schenker, M. A., Robertson, B. E., Ellis, R. S., *et al.* 2013, *ApJ*, 768, 196
Schmidt, K. B., Treu, T., Brammer, G. B., *et al.* 2014, *ApJL*, 782, L36
Sharon, K., Gladders, M. D., Rigby, J. R., *et al.* 2012, *ApJ*, 746, 161
Smit, R., Bouwens, R. J., Labbé, I., *et al.* 2014, *ApJ*, 784, 58
Smit, R., Swinbank, A. M., Massey, R., Richard, J., Smail, I., Kneib, J.-P., *et al.* 2017, *MNRAS*, 467, 3306
Sparre, M., Hayward, C. C., Feldmann, R., *et al.* 2017, *MNRAS*, 466, 88
Sparre, M., Hayward, C. C., Springel, V., *et al.* 2015, *MNRAS*, 447, 3548
Speagle, J. S., Steinhardt, C. L., Capak, P. L., & Silverman, J. D. 2014, *ApJS*, 214, 15
Stark, D. P., Schenker, M. A., Ellis, R., *et al.* 2013, *ApJ*, 763, 129
Straughn, A. N., Kuntschner, H., Kümmel, M., *et al.* 2011, *AJ*, 141, 14
Tacchella, S., Dekel, A., Carollo, C. M., *et al.* 2016, *MNRAS*, 457, 2790
Torrey, P., Vogelsberger, M., Genel, S., *et al.* 2014, *MNRAS*, 438, 1985
Trebitsch, M., Blaizot, J., Rosdahl, J., Devriendt, J., & Slyz, A. 2017, *MNRAS*, 470, 224
Weisz, D. R., & Boylan-Kolchin, M. 2017, *MNRAS*, 469, L83
Weisz, D. R., Dolphin, A. E., Skillman, E. D., *et al.* 2014, *ApJ*, 789, 148
Weisz, D. R., Johnson, B. D., & Conroy, C. 2014, *ApJL*, 794, L3
Whitaker, K. E., van Dokkum, P. G., Brammer, G., & Franx, M. 2012, *ApJL*, 754, L29
Yue, B., Ferrara, A., Vanzella, E., & Salvaterra, R. 2014, *MNRAS*, 443, L20
Zheng, W., Shu, X., Moustakas, J., *et al.* 2014, *ApJ*, 795, 93